J Mater Sci (2020) 55:2741–2749

Ceramics

Structure and chemical durability studies of powellite ceramics $Ca_{1-x}Li_{x/2}Gd_{x/2}MoO_4$ ($0 \le x \le 1$) for radioactive waste storage

Cheng Meng[1,2], Wenqi Li[2,3,*], Chunrong Ren[2], and Junchuan Zhao[2]

[1] Jiangxi Province Key Laboratory of Polymer Micro/Nano Manufacturing and Devices, School of Chemistry, Biology and Materials Science, East China University of Technology, Nanchang 330013, People's Republic of China
[2] Department of Materials Science and Engineering, Zhejiang University, Hangzhou 310027, People's Republic of China
[3] R&D Centre, Jinko Solar Co., Ltd., Haining 314400, People's Republic of China

Received: 22 July 2019
Accepted: 13 November 2019
Published online: 2 December 2019

ABSTRACT

Powellite ceramic represents a waste form matrix material to immobilize minor actinides and Mo from reprocessed UMo nuclear fuel. In this paper, the $Ca_{1-x}Li_{x/2}Gd_{x/2}MoO_4$ ($0 \le x \le 1$) series is prepared by solid-state reaction using Gd^{3+} as trivalent minor actinide (Cm^{3+}) surrogate, and the structure/microstructure is characterized by XRD, HRTEM, Raman spectroscopy and SEM. Rietveld refinements show that the couple (Gd^{3+} and Li^{+}) enters into the eightfold coordinated Ca site of the powellite structure. With the increase in the contents of Gd and Li, Raman bands broaden due to the distortion of MoO_4 tetrahedra and disordered arrangements of Gd^{3+} and Li^{+}. The chemical durability analyzed by the PCT-B indicates that the leaching behaviors of Gd and Mo are related to the interfacial dissolution–reprecipitation mechanism. For the $Ca_{0.5}Li_{0.25}Gd_{0.25}MoO_4$ ceramic, 7-day NL_{Gd} and NL_{Mo} are shown in the order of $\sim 10^{-4}$ and $\sim 10^{-4}$ g m^{-2}, respectively. Thus, our initial results of the structure and chemical durability will provide insights to design new single- or multiphase waste forms for the Mo-rich HLW conditioning.

Introduction

The high-level wastes (HLWs) stored in large underground steel tanks have been accumulating from reprocessed nuclear fuel [1]. Due to the long-term radiotoxic of radioisotopes existing in the HLWs, such storage is acceptable for few years and exerts an ever-increasing threat to the biosphere. Thus, these wastes must be immobilized in non-dispersible and leach-resistant matrix, stored and disposed off within suitable geological repositories [1–3]. For UMo HLWs containing a high concentration of molybdenum, borosilicate glassy matrices have been developed to immobilize molybdenum, other fission products and actinides. Researches on the solubility of Mo within borosilicate glass melts

Address correspondence to E-mail: liwq@zju.edu.cn

https://doi.org/10.1007/s10853-019-04223-y

indicate that is relatively low (~ 1 wt% MoO_3), which limits the amount of waste loading (15–20 wt%) [4, 5]. Moreover, borosilicate glass waste form accompanies the shortcoming of phase separation on melting and can crystallize simultaneously with poorly durable Na_2MoO_4 and more durable $CaMoO_4$ (powellite) phases [6–8]. In this regard, significant efforts are being made to incorporate Mo, other fission products and actinides in a highly stable and durable ceramic matrix. The main ceramic phases considered for immobilization of theses nuclides are sodium zirconium phosphate (NZP) [9–11], monazite [12, 13], powellite [14, 15], etc.

Molybdenum is a multivalent element and can exist as + 4 or + 6 oxidation state in the compounds [16]. Tetravalent and hexavalent Mo can enter either octahedral (Oh) position L or tetrahedral (Td) position T of the NZP framework, likely $NaMo_2(PO_4)_3$, $AMo_2P_3O_{12}$ (A = K, Rb, Ti) and $AMo_2(PO_4)_3$ (A = Ba, Sr, Ca) compounds [17–19]. However, the NZP structure for the immobilization of Mo (IV) is not stable under air atmosphere because tetravalent Mo can be easily oxidized [10]. An attempt has been made to introduce Mo as +6 oxidation state in monazite waste forms with $La_{1-x}Ca_xP_{1-y}MoO_4$ (x = y = 0.1–0.9) compositions, which can crystallize in either monazite or scheelite structure depending on the level of Mo (VI) substitution [12]. The chemical durability of monazite waste form $La_{0.4}Nd_{0.1}Y_{0.1}$-$Gd_{0.1}Sm_{0.1}Ce_{0.1}Ca_{0.1}P_{0.9}Mo_{0.1}O_4$ has been tested through dynamic MCC-5 method, and the leach rate of molybdenum is found to be in the order of 10^{-3}–10^{-4} g m^{-2} d^{-1} [13].

Powellite (nominally, $CaMoO_4$), which crystallizes in the scheelite-type tetragonal structure (space group $I4_1/a$, Z = 4), consists of CaO_8 polyhedron and MoO_4 tetrahedron sharing common vertices and can be visualized as the assembly of columns made up by –CaO_8–MoO_4–CaO_8–MoO_4– along c-axis [20, 21]. The polyhedral view of the powellite structure is shown in Fig. 1. Based on the structural flexibility, the powellite structure can accommodate considerable trivalent actinides. Until now to our knowledge, previous researches, which mainly employ the formation of powellite phase during glass composite materials processing, are investigated as a component in the multiphase waste forms [7, 15, 22–26]. However, limited work focuses on the relation between structure and property of single-phase powellite materials [15, 21, 27]. For instance, the chemical

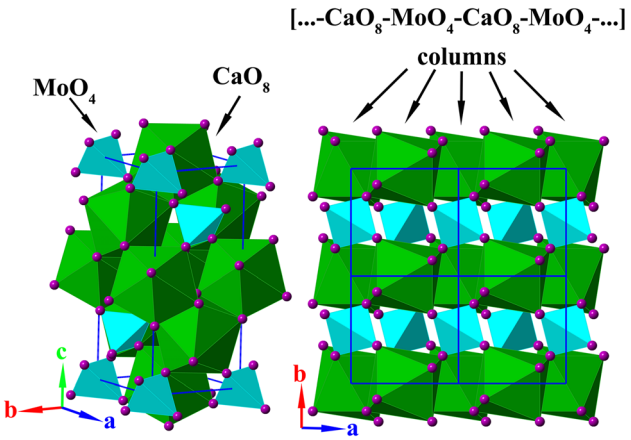

Figure 1 Polyhedral view (left) and ab projection of the powellite-type structure (right). Magenta spheres are oxygen anions.

durability of powellite $CaMoO_4$ has been investigated using the PCT-B. The present work shows low normalized release rates for Ba, Ca and Mo, suggesting high chemical durability [15]; however, little information is known regarding the leaching behavior of actinides incorporated in the powellite structure. A systematic investigation of structure and aqueous durability of powellite materials can provide useful information for understanding current and future single- or multiphase waste forms.

To close this gap, the immobilization of actinides in single-phase powellite ceramics and chemical durability of the corresponding waste forms are investigated in this paper. According to the isomorphism theory, Gd^{3+} is used to mimic trivalent curium (Cm). Thus, a series of ceramics $Ca_{1-x}Li_{x/2}Gd_{x/2}MoO_4$ ($0 \le x \le 1$) are prepared by a solid-state reaction process. The effect of the nature of minor actinide surrogate (Gd) on the structure in the $Ca_{1-x}Li_{x/2}Gd_{x/2}MoO_4$ system is undertaken, with leaching behaviors of Gd and Mo analyzed by PCT-B as well.

Experimental

Preparation of samples

Ceramics with the general formula $Ca_{1-x}Li_{x/2}Gd_{x/2}MoO_4$ ($0 \le x \le 1$) are synthesized by conventional solid-state reaction of the starting reactants, $CaCO_3$ (Macklin and purity > 99%), Gd_2O_3 (Aladdin and purity > 99%), Li_2CO_3 (Aladdin and purity > 99%) and Mo_2O_3 (Aladdin and purity > 99%). The

corresponding stoichiometric compositions of powders are milled on the planetary milling machine (Nanjing Machine Factory, China) at 300 rpm for 4 h using anhydrous ethanol as the milling media and calcined at 500 °C for 3 h. The obtained slurries are dried at 90 °C for 24 h, calcined in air at 500 °C for 3 h and milled for 4 h afterward. Subsequently, the homogeneous powders are dried, granulated with 5 wt% PVA and pressed into cylinders (15 mm in diameter and 4–5 mm in height) under a uniaxial pressure of 200 MPa. Finally, these cylinders are sintered from 525 to 950 °C for 3 h in the ambient atmosphere.

X-ray diffraction (XRD)

The crystalline structures of the sintered products are investigated by X-ray diffraction analysis with Cu K_α radiation (PANalytical X'pert PRO diffractometer). The XRD data are collected over the 2θ ranging from 10° to 120° with steps of 0.02°. The structural parameters are analyzed with the Rietveld refinement method using the FullProf package [28].

HRTEM, SEM and Raman spectroscopy

The high-resolution transmission electron microscopy (HRTEM) is performed using a Tecnai G2 F20 S-TWIN FEI transmission electron microscope operating at 200 kV. Microstructures of platinum coated samples are observed using a Hitachi S-3700 N scanning electron microscopy (SEM). Raman spectra at room temperature are collected with a microspectrometer DXR SmartRaman (Thermo Fisher) excited by an argon laser at 514.5 nm.

Dissolution study

The chemical durability of ceramics is examined by the ASTM C1285-14 product consistency test method B (PCT-B) [29]. In the test method, samples are crushed and sieved to isolate the size fraction of the USA (Standard ASTM (100–200 mesh)). Three grams of cleaned particles is placed in a 60-ml polytetrafluoroethylene (PTFE) vessel. An amount of deionized water equal to 30 ml is added, and the PTFE vessel is sealed. The PTFE vessel is placed in a constant temperature device at 90 °C. After different leaching times, the concentrations of the released Gd and Mo are measured with inductively coupled plasma mass spectrometry (ICP-MS) using XSENIES apparatus. From ICP-MS results, normalized elemental mass losses of gadolinium and molybdenum are determined by the equation derived from PCT-B [29]. To analyze the differences between microstructures at longer leaching durations, the deionized water in the testing vessel is renewed at every 28-day test.

Results and discussion

XRD and HRTEM analyses

To investigate the optimal condition for the preparation of powellite ceramics with $Ca_{1-x}Li_{x/2}Gd_{x/2}MoO_4$ ($0 \le x \le 1$) compositions, the typical composition $Ca_{0.5}Li_{0.25}Gd_{0.25}MoO_4$ is heated at several temperatures ranging from 525 to 950 °C. Analytic results of the corresponding XRD patterns are shown in Fig. 2. At 525 °C, the crystalline phases of the sample are $CaMoO_4$ (JCPDS file no. 85-0546), Gd_2O_3 (JCPDS file no. 88-2165) and $Li_2Mo_4O_{13}$ (JCPDS file no. 25-0494). Between 525 and 550 °C, the intensities of the peaks of Gd_2O_3 and $Li_2Mo_4O_{13}$ phases decrease, while those of $CaMoO_4$ phase increase. This indicates that the isomorphism of powellite forms during the increase in the sintering temperature. At 600 °C, the XRD patterns are indexed to the single-phase powellite with $Ca_{0.5}Li_{0.25}Gd_{0.25}MoO_4$ composition, due to the disappearance of the XRD lines from $CaMoO_4$, Gd_2O_3 and $Li_2Mo_4O_{13}$ phases. Above 600 °C, the crystallinity of the powellite ceramic $Ca_{0.5}Li_{0.25}Gd_{0.25}MoO_4$ is widely improved, which is determined by the average full width at the half maximum (FWHM) of the main XRD lines, corresponding to the 011, 112, 004, 020, 211, 114, 024, 020 and 116 peaks. The average FWHM of these peaks, which are obtained at 600, 650, 700, 750, 800, 850 and 900 °C, are found to be 0.251, 0.212, 0.203, 0.193, 0143, 0.145 and 0.140 °, respectively (Fig. 3). From the FWHM, it can be deduced that the optimized temperature for the synthesis of the powellite-type $Ca_{1-x}Li_{x/2}Gd_{x/2}MoO_4$ ($0 \le x \le 1$) solid solution is over 800 °C.

To examine the effect of the minor actinide surrogate (Gd) content on the structure in the $Ca_{1-x}Li_{x/2}Gd_{x/2}MoO_4$ system, the $Ca_{1-x}Li_{x/2}Gd_{x/2}MoO_4$ ($0 \le x \le 1$) compositions are sintered at 850 °C and corresponding powder XRD patterns are shown in Fig. 4. The XRD investigation shows that

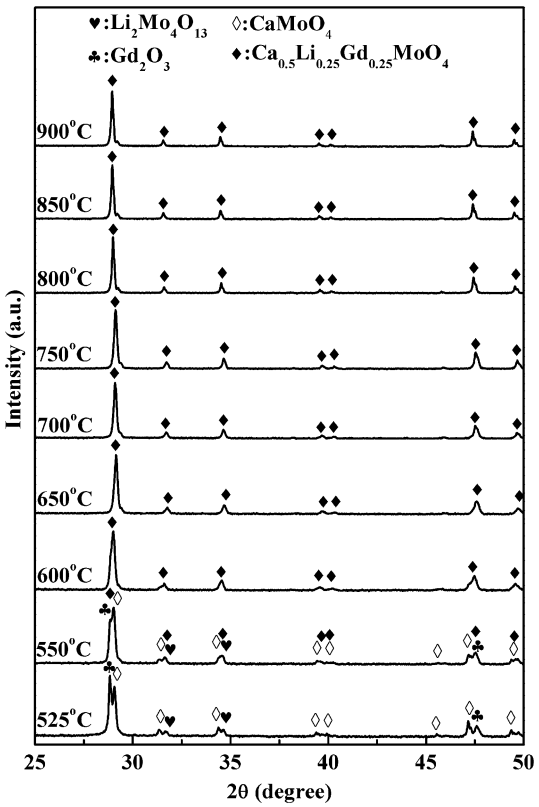

Figure 2 XRD analysis of Gd_2O_3–$CaCO_3$–Mo_2O_3–Li_2CO_3 mixture calcined at several temperatures.

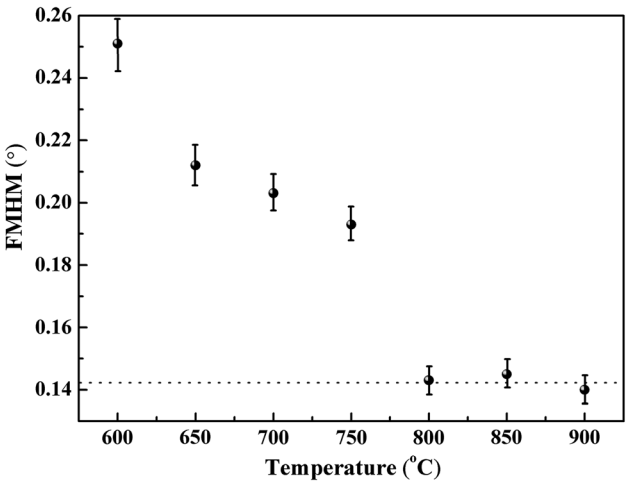

Figure 3 Average FWHM obtained from main XRD lines of $Ca_{0.5}Li_{0.25}Gd_{0.25}MoO_4$ composition versus the sintering temperature.

$Ca_{1-x}Li_{x/2}Gd_{x/2}MoO_4$ $(0 \le x \le 1)$ compositions crystallize in the scheelite-type structure, and intense reflections of powellite phases observed in the range from 10° to 65° are indexed to (011), (112), (004), (020), (211), (114), (024), (200), (116), (312) and (224), respectively. Meanwhile, Rietveld refinement is performed on all of these compounds. Since Li element has a very low atomic number relative to the other elements in the powellite phases and a conventional Cu anode is used to collect the diffraction patterns, structural model including or without Li is used to evaluate the confidence of the refinement result. The agreement factors for the refined model including Li with representative composition $Ca_{0.6}Li_{0.2}Gd_{0.2}MoO_4$ are: R_p = 14.4%, R_{wp} = 9.52%, R_B = 2.38% and R_F = 2.49, S = 1.77; those for the initial model without Li are R_p = 14.9%, R_{wp} = 10.02%, R_B = 2.67%, R_F = 2.74% and S = 1.89. Compared with these values, it is found that the refinement of the structural model with Li atoms is credible due to its smaller agreement factors. As a result, final refinement plots of $Ca_{0.6}Li_{0.2}Gd_{0.2}MoO_4$ composition are presented in Fig. 5, and the corresponding atomic parameters are shown in Table 1. It is clear that the couple (Gd^{3+}, Li^+) enters the eightfold coordinated Ca site of the scheelite-type structure (Table 1). The analysis of the

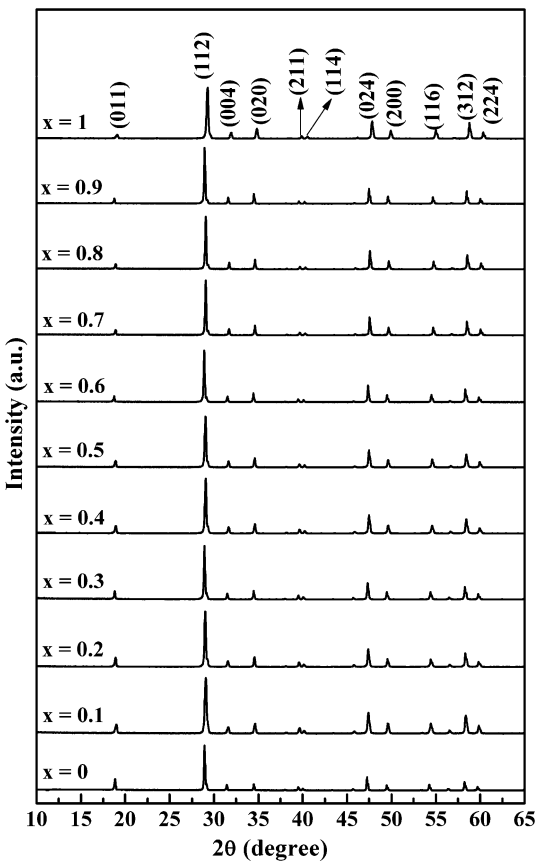

Figure 4 Representative XRD patterns of $Ca_{1-x}Li_{x/2}Gd_{x/2}MoO_4$ $(0 \le x \le 1)$ powellite solid solutions.

unit cell parameters given in Table 2 indicates that a noticeable decrease occurs in the compositions $0 \leq x \leq 1$. The result can be attributed to the increase in x with the decrease in average cationic radii in the eightfold coordination of Ca site. According to the Shannon's data [30], the equivalent radii of Ca site for the $Ca_{1-x}Li_{x/2}Gd_{x/2}MoO_4$ ceramics are $r = 1.12 - 0.1335x$ (Ion radius of Gd^{3+}, Li^+ and Ca^{2+} is 1.053 Å, 0.92 Å and 1.12 Å, respectively). In addition, the value of a/c increases with the increase in the x value.

To further understand the resulting phases of the $Ca_{1-x}Li_{x/2}Gd_{x/2}MoO_4$ compositions, the samples are characterized by HRTEM. For the sake of briefness, only HRTEM result of powellite ceramic with $Ca_{0.6}Li_{0.2}Gd_{0.2}MoO_4$ composition is presented, as shown in Fig. 6. The observed zone of $Ca_{0.6}Li_{0.2}Gd_{0.2}MoO_4$ particles displays clear lattice fringes. Analyses of interplanar spacing of (022) and (020) planes along [400] axis are found to be 0.237 and 0.261 nm, respectively, which are in good agreement with Rietveld refinement results.

Raman spectra study

Previous group theory calculations have suggested that powellite ($CaMoO_4$) crystal has 26 vibrations of species ($\Gamma = 3A_g + 5A_u + 5B_g + 3B_u + 5E_g + 5E_u$), where $3A_g$, $5B_g$ and $5E_g$ are 13 Raman active vibrations, $4A_u$ and $4E_u$ are eight infrared active vibrations and $3B_u$ are three silent vibrations [31–33]. Raman active modes in the structure also can be divided into internal and external vibrational modes. The internal modes are associated with the oscillations inside the $[MoO_4]^{2-}$ molecular group with a stationary mass center. The external modes, which are composed of rotation and translation modes, are related to the motion of A^{2+} cation and the rigid molecular units [32].

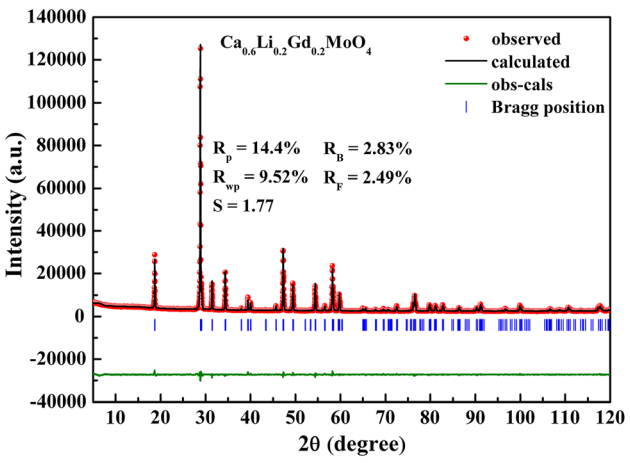

Figure 5 Rietveld refinement plots of $Ca_{0.6}Li_{0.2}Gd_{0.2}MoO_4$ composition showing the observed (o), calculated (solid line), difference pattern (lower) and the positions of allowed Bragg reflections (vertical lines).

The spectroscopic characterizations of some representative $Ca_{1-x}Li_{x/2}Gd_{x/2}MoO_4$ ($0 \leq x \leq 0.9$) compositions through Raman experiments in the frequency range of 100–1200 cm^{-1} are shown in Fig. 7. The internal mode frequencies range from 305 to 900 cm^{-1}, whereas external mode frequencies are below 305 cm^{-1}. The high-frequency vibration Raman line around 879 cm^{-1} corresponds to the symmetric stretching vibration $v_1(A_g)$. Peaks observed at 795 and 848 cm^{-1} are associate with the stretching motions which can be assigned as $v_3(E_g)$ and $v_3(B_g)$, respectively. Raman lines centered at 392 [$v_4(B_gE_g)$] and 407 [$v_4(B_gE_g)$] cm^{-1} belong to symmetric bending vibration. The Raman frequency located at 325 cm^{-1} presents the asymmetric bending mode $v_2(A_gB_g)$. Further, the Raman frequency located at 114 and 206 cm^{-1} is associated with the rotational and translational modes. For all the internal vibrational modes, Raman bands broaden with the increase in the level of Gd and Li substitution, while the change in the intensity reverses. These phenomena may result from the distortion of the MoO_4 tetrahedra [33, 34]. When the proportion of Gd^{3+} and Li^{1+} ions on the Ca site increases, the MoO_4 may appear more distorted on the local scale. As a result, the regular change in the internal vibration modes can be observed. Compared with the internal modes, the evolution of the external modes versus x values follows the same trend. This interesting result is related to the distortion of MoO_4 tetrahedra and disordered arrangements of Gd^{3+} and Li^+ [20, 33, 35].

Durability assessment

To assess the leaching behaviors of minor actinide surrogate (Gd) and Mo in powellite ceramics, PCT-B is performed on the selected composition $Ca_{0.5}Li_{0.25}Gd_{0.25}MoO_4$. The normalized releases of Gd and Mo for different leaching times are presented in Table 3, and corresponding plots are shown in Fig. 8. As shown in Fig. 8, the initial rapid releases of Gd and Mo occur during the leaching test. For 3-h leaching,

Table 1 Structural parameters of the $Ca_{0.6}Li_{0.2}Gd_{0.2}MoO_4$ ceramic

Atoms	Wyckoff site	x	y	z	Occupancies	Isotropic thermal parameters
Ca1	4b	0.0000	0.2500	0.6250	0.6	0.57(4)
Li1	4b	0.0000	0.2500	0.6250	0.2	0.57(4)
Gd1	4b	0.0000	0.2500	0.6250	0.2	0.57(4)
Mo1	4a	0.0000	0.2500	0.1250	1.0	0.65(1)
O1	16f	0.2406(4)	0.0993(5)	0.0399(2)	1.0	0.73(1)

Table 2 Summary of phases identified in $Ca_{1-x}Li_{x/2}Gd_{x/2}MoO_4$ ($0 \le x \le 1$) ceramics and their unit parameters

x	Phases	a (Å)	c (Å)	V $(Å)^3$	a/c
0	Powellite	5.2282(1)	11.4446(2)	312.83(1)	0.4568(2)
0.1	Powellite	5.2267(1)	11.4306(7)	312.27(2)	0.4572(5)
0.2	Powellite	5.2218(1)	11.4104(4)	311.13(2)	0.4576(3)
0.3	Powellite	5.2189(1)	11.3977(4)	310.44(2)	0.4578(9)
0.4	Powellite	5.2168(1)	11.3848(4)	309.84(1)	0.4582(2)
0.5	Powellite	5.2161(2)	11.3778(5)	309.57(2)	0.4584(4)
0.6	Powellite	5.2043(1)	11.3468(3)	307.32(1)	0.4586(5)
0.7	Powellite	5.2030(1)	11.3398(4)	306.99(1)	0.4588(2)
0.8	Powellite	5.1980(2)	11.3248(4)	305.99(2)	0.4589(9)
0.9	Powellite	5.1916(1)	11.3084(3)	304.79(1)	0.4590(9)
1.0	Powellite	5.1925(2)	11.3064(6)	304.84(2)	0.4592(5)

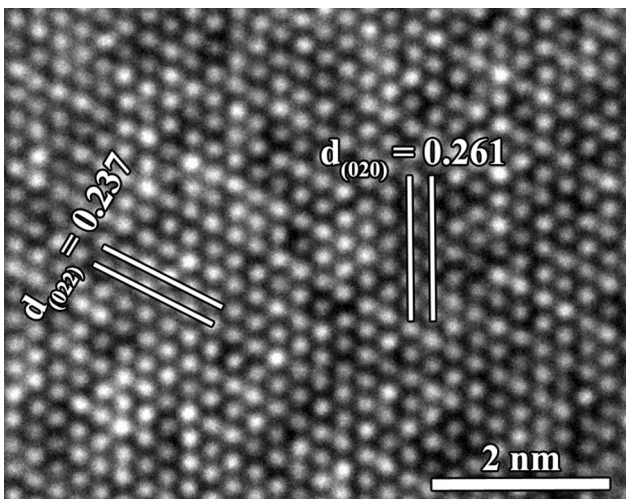

Figure 6 HRTEM image of $Ca_{0.6}Li_{0.2}Gd_{0.2}MoO_4$ particles along the [400] zone with (022) and (020) planes.

the NL_{Gd} and NL_{Mo} reach the maximum values of 5.28×10^{-2} and 2.87×10^{-2} g m^{-2}, respectively (Table 3). With the increase in leaching time, the normalized releases decrease and attain a near-equilibrium condition after 7 days (Fig. 8). For leaching

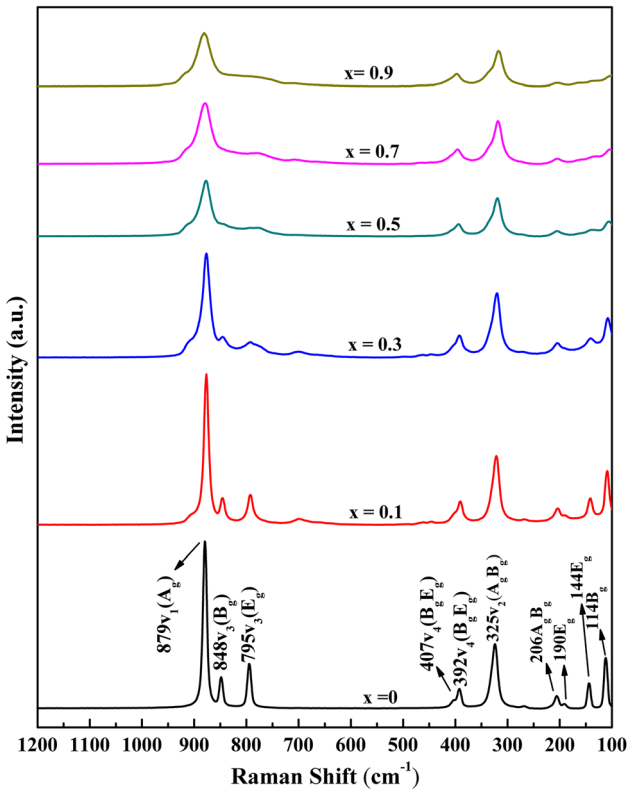

Figure 7 Representative Raman spectroscopy of $Ca_{1-x}Li_{x/2}Gd_{x/2}MoO_4$ ($0 \le x \le 0.9$) ceramics.

times ranging from 7 to 28 days, the NL_{Gd} and NL_{Mo} are shown in the order of $\sim 10^{-4}$ and $\sim 10^{-4}$ g m^{-2}, respectively (Table 3). These results indicate that powellite ceramics exhibit the great retention of Gd and Mo.

Based on the above description, the leaching behaviors can be explained by the interfacial dissolution–reprecipitation mechanism [36–39]. In this situation, the whole leaching process can be divided into three stages. The first stage is from 0 to 3 h, in which Gd(III) and Mo (VI) from superficial surfaces are quickly dissolved in water and form hydrolyzed species on the reaction interfaces subsequently. The

Table 3 Normalized releases of Gd and Mo from $Ca_{0.5}Li_{0.25}Gd_{0.25}MoO_4$ ceramic for different time durations

Normalized releases	3 h	8 h	3 d	5 d	7 d	14 d	28 d
NL_{Gd} (10^{-4} g m^{-2})	528.89	167.27	42.08	45.55	9.40	1.18	1.38
NL_{Mo} (10^{-4} g m^{-2})	2868.78	397.84	25.78	15.80	4.08	5.11	2.21

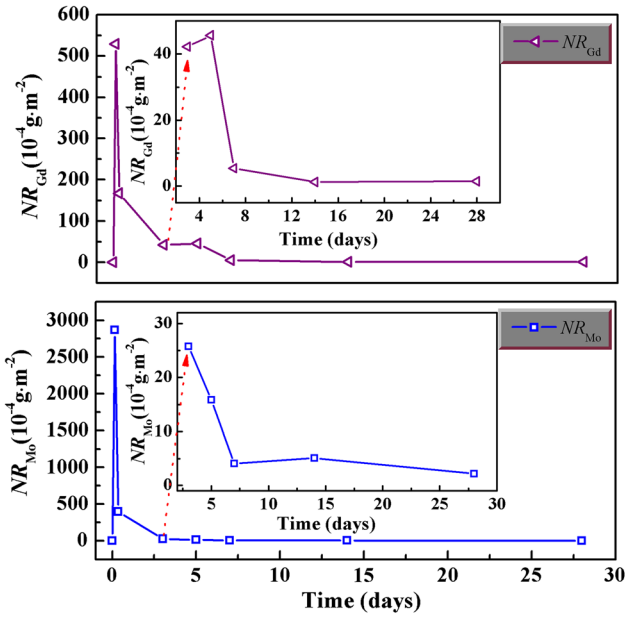

Figure 8 Evolution of Gd- and Mo-normalized releases of the $Ca_{0.5}Li_{0.25}Gd_{0.25}MoO_4$ ceramic versus leaching duration.

second stage is from 3 h to 7 days. In this leaching period, the hydrolyzed species consistently form precipitation phases and cover on the surface of the $Ca_{0.5}Li_{0.25}Gd_{0.25}MoO_4$ particles which reduce the NL_{Gd} and NL_{Mo}. For the final stage with longer leaching times ranging from 7 to 28 days, the inner immobilized Gd and Mo elements hardly escape from the matrix due to the long pathways. Meanwhile, the formation and reprecipitation of hydrolyzed species reach the dynamic equilibrium leading to the invariant magnitude of NL_{Gd} and NL_{Mo}. These results are further verified by the microstructure of the $Ca_{0.5}Li_{0.25}Gd_{0.25}MoO_4$ ceramic after leaching 90 days, as shown in Fig. 9. The clear surface of the sample without leaching test is observed, whereas small particles observed on the surface after leaching 90 days suggest that the formation of precipitate phases occurs during the dissolution test. The observations of SEM are consistent with the leaching behaviors of minor actinide surrogate (Gd) and Mo. Unfortunately, such precipitates cannot be determined by EDS due to the contents below the instrumental detection limits. All the results indicate that powellite ceramics can be used as a promising candidate waste form for the conditioning of minor actinide and Mo.

Conclusions

The aim of this work was to investigate the structure and leaching behavior in the $Ca_{1-x}Li_{x/2}Gd_{x/2}MoO_4$ ($0 \le x \le 1$) system. The main conclusions drawn from this paper are the following:

(i) The preparation of the powellite-type $Ca_{1-x}Li_{x/2}Gd_{x/2}MoO_4$ ($0 \le x \le 1$) solid solution requires sintering temperature over 800 °C. For all the $Ca_{1-x}Li_{x/2}Gd_{x/2}MoO_4$ ceramics, the

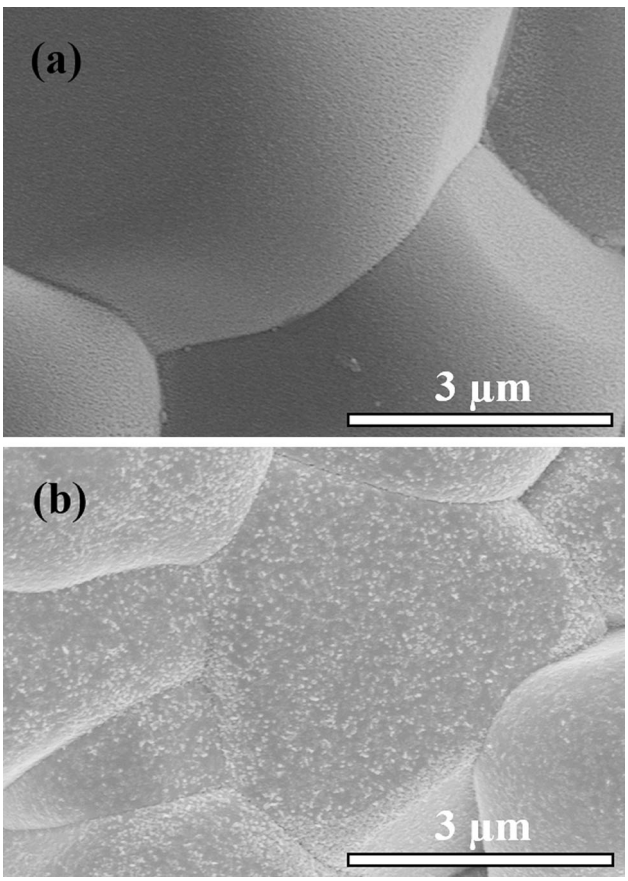

Figure 9 SEM images of $Ca_{0.5}Li_{0.25}Gd_{0.25}MoO_4$ ceramic **a** before leaching and **b** after 90 days of leaching in initially pure water at 90 °C.

couple (Gd^{3+}, Li^{+}) is incorporated in the eightfold coordinated Ca site of the scheelite-type structure. The evolution of cell parameters decreases with the increase in x. The change in the peaks of Raman spectra is relevant to the distortion of MoO_4 tetrahedra and the disordered arrangements of Gd^{3+} and Li^{+}.

(ii) The ceramic with $Ca_{0.5}Li_{0.25}Gd_{0.25}MoO_4$ composition exhibits the great retention of Gd and Mo; 7-day NL_{Gd} and NL_{Mo} are found to be in the order of $\sim 10^{-4}$ and $\sim 10^{-4}$ g m^{-2}, respectively. The leaching behaviors of minor actinide surrogate (Gd) and Mo in the powellite ceramics are attributed to the interfacial dissolution–reprecipitation mechanism.

Acknowledgements

The authors would like to thank the editor and the anonymous reviewers for their valuable comments on this manuscript. All authors contributed to the discussion of the results and preparation of the manuscript. The present work was supported by the Fundamental Research Funds for the Central Universities of Zhejiang University (CN).

Compliance with ethical standards

Conflict of interest There are no conflicts to declare.

References

[1] Sengupta P (2012) A review on immobilization of phosphate containing high level nuclear wastes within glass matrix—present status and future challenges. J Hazard Mater 235:17–28

[2] Donald IW, Metcalfe BL, Taylor RNJ (1997) The immobilization of high level radioactive wastes using ceramics and glasses. J Mater Sci 32:5851–5887. https://doi.org/10.1023/A:1018646507438

[3] Crum JV, Turo L, Riley B et al (2012) Multi-phase glass-ceramics as a waste form for combined fission products: alkalis, alkaline earths, lanthanides, and transition metals. J Am Ceram Soc 95:1297–1303

[4] Johnson LH, Shoesmith DW, Lutze W et al (1988) Radioactive waste forms for the future. North Holland, Amsterdam

[5] Szumera M, Wacławska I (2012) Effect of molybdenum addition on the thermal properties of silicate-phosphate glasses. J Therm Anal Calorim 109:649–655

[6] Asfari Z, Bressot C, Vicens J et al (1995) Doubly crowned calix[4]arens in the 1, 3-alternate conformation as cesium-selective carriers in supported liquid membranes. Anal Chem 67:3133–3139

[7] Kossoy A, Schulze R, Tang M et al (2013) Nd–Mo-borosilicate glass-ceramic: synthesis, characterization and response to ionizing radiation. J Nucl Mater 437:216–221

[8] Hyatt NC, Short RJ, Hand RJ et al (2005) The structural chemistry of molybdenum in model high level nuclear waste glasses, investigated by Mo K-edge X-ray absorption spectroscopy. Ceram Trans 168:179–187

[9] Chourasia R, Shrivastava OP, Wattal PK (2009) Synthesis, characterization and structure refinement of sodium zirconium molibdo-phosphate: $Na_{0.9}Zr_2Mo_{0.1}P_{2.9}O_{12}$ (MoNZP). J Alloys Compd 473:579–583

[10] Pet'kov VI, Sukhanov MV, Kurazhkovskaya VS (2003) Molybdenum fixation in crystalline NZP matrices. Radiochemistry 45:620–625

[11] Dahale ND, Keskar M, Sali SK et al (2008) Preparation and characterisation of $Tl_2Pu(MoO_4)_3$ and $Tl_4Pu(MoO_4)_4$ in Tl–Pu–Mo–O system by X-ray and thermal methods. J Nucl Mater 376:129–132

[12] Kumar SP, Gopal B (2011) Immobilization of "Mo^{6+}" in monazite lattice: synthesis and characterization of new phosphomolybdates, $La_{1-x}Ca_xP_{1-y}MoyO_4$, where x = y = 0.1 - 0.9. J Am Ceram Soc 94:1008–1013

[13] Pratheep Kumar S, Gopal B (2015) Simulated monazite crystalline wasteform $La_{0.4}Nd_{0.1}Y_{0.1}Gd_{0.1}Sm_{0.1}Ce_{0.1}Ca_{0.1}(-P_{0.9}Mo_{0.1}O_4)$: synthesis, phase stability and chemical durability study. J Nucl Mater 458:224–232

[14] Stewart MWA, Vance ER (2006) Waste form strategies for Mo-rich radioactive waste. WM' 06 conference, Tucson, AZ

[15] Brinkman K, Fox K, Marra J et al (2013) Single phase melt processed powellite (Ba, Ca)MoO_4 for the immobilization of Mo-rich nuclear waste. J Alloys Compd 551:136–142

[16] Caurant D, Majérus O, Fadel E et al (2007) Effect of molybdenum on the structure and on the crystallization of SiO_2–Na_2O–CaO–B_2O_3 glasses. J Am Ceram Soc 90:774–783

[17] Lii KH, Chen JJ, Wang SL (1989) $NaMo_2P_3O_{12}$: a new phosphate of Mo(IV). J Solid State Chem 78:93–97

[18] Leclaire A, Raveau B (1988) Small atomic displacements in the molybdenophosophates $AMo_2P_3O_{12}$ (A = K, Rb, Ti). Acta Crystallogr Sect C: Cryst Struct Commun 44:226–229

[19] Leclaire AB, Borel MM, Grandin A et al (1989) A novel family of mixed valence molybdenum phosphate with a

nasicon structure, $AMo_2P_3O_{12}$ (A = Ca, Sr, Ba). Eur J Solid State Inorg Chem 26:45–51

[20] Rabuffetti FA, Culver SP, Leopoldo S et al (2014) Structural disorder in $AMoO_4$ (A = Ca, Sr, Ba) scheelite nanocrystals. Inorg Chem 53:1056–1061

[21] Achary SN, Patwe SJ, Mathews MD et al (2006) High temperature crystal chemistry and thermal expansion of synthetic powellite ($CaMoO_4$): a high temperature X-ray diffraction (HT-XRD) study. J Phys Chem Solids 67:774–781

[22] Short RJ, Hand RJ, Hyatt NC et al (2005) Environment and oxidation state of molybdenum in simulated high level nuclear waste glass compositions. J Nucl Mater 340:179–186

[23] Bosbach D, Luckscheiter B, Brendebach B et al (2009) High level nuclear waste glass corrosion in synthetic clay pore solution and retention of actinides in secondary phases. J Nucl Mater 385:456–460

[24] Vance ER, Davis J, Olufson K et al (2014) Leaching behaviour of and Cs disposition in a UMo powellite glass-ceramic. J Nucl Mater 448:325–329

[25] Ohkubo T, Monden R, Iwadate Y et al (2015) Structural investigation of aluminoborosilicate glasses containing Na_2MoO_4 crystallites by solid state NMR. Phys Chem Glasses B 56:139–144

[26] Taurines T, Boizot B (2012) Microstructure of powellite-rich glass-ceramics: a model system for high level waste immobilization. J Am Ceram Soc 95:1105–1111

[27] Bosbach D, Rabung T, Brandt F et al (2004) Trivalent actinide coprecipitation with powellite ($CaMoO_4$): secondary solid solution formation during HLW borosilicate-glass dissolution. Radiochim Acta 92:639–643

[28] Rodriguez-Carjaval J (1993) The programs for rietveld refinement. Phys B 192:55–69

[29] ASTM (2014) Standard test methods for determining chemical durability of nuclear, hazardous, and mixed waste glasses and multiphase glass ceramics: the product consistency test (PCT)

[30] Shannon RD (1976) Revised effective ionic-radii and systematic studies of interatomic distances in halides and chalcogenides. Acta Crystallogr 32:751–767

[31] Porto SPS, Scott JF (1967) Raman spectra of $CaWO_4$ $SrWO_4$ $CaMoO_4$ and $SrMoO_4$. Phys Rev 157:716–729

[32] Basiev TT, Sobol AA, Voronko YK et al (2000) Spontaneous Raman spectroscopy of tungstate and molybdate crystals for Raman lasers. Opt Mater 15:205–216

[33] Xi H, Di Z, Xie H et al (2015) Raman spectra, infrared spectra, and microwave dielectric properties of low-temperature firing $[(Li_{0.5}Ln_{0.5})_{1-x}Ca_x]MoO_4$ (Ln = Sm and Nd) solid solution ceramics with scheelite structure. J Am Ceram Soc 98:587–593

[34] Hao S, Zhou D, Pang L (2019) The spectra analysis and microwave dielectric properties of $[Ca_{0.55}(Sm_{1-x}Bi_x)_{0.3}]$-$MoO_4$ ceramics. J Am Ceram Soc 102:3103–3109

[35] Munirathnappa AK, Dwibedi D, Hester J et al (2019) In situ neutron diffraction studies of $LiCe(WO_4)_2$ polymorphs: phase transition and structure-property correlation. J Phys Chem C 123:1041–1049

[36] Danelska A, Ulkowska U, Socha RP et al (2013) Surface properties of nanozirconia and their effect on its rheological behaviour and sinterability. J Eur Ceram Soc 33:1875–1883

[37] Fillet C, Advocat T, Bart F et al (2004) Titanate-based ceramics for separated long-lived radionuclides. C R Chim 7:1165–1172

[38] Zhang L, Lüttge A (2009) Theoretical approach to evaluating plagioclase dissolution mechanisms. Geochim Cosmochim Acta 73:2832–2849

[39] Li W, Ding X, Meng C et al (2018) Phase structure evolution and chemical durability studies of $Gd_{1-x}Yb_xPO_4$ ceramics for immobilization of minor actinides. J Mater Sci 53:6366–6377. https://doi.org/10.1007/s10853-018-2031-z